Published in final edited form as:
Cancer Discov. 2014 February ; 4(2): 200–215. doi:10.1158/2159-8290.CD-13-0235.

MEK-Dependent Negative Feedback Underlies BCR-ABL-Mediated Oncogene Addiction

Jennifer Asmussen[1], **Elisabeth A. Lasater**[2,*], **Cheryl Tajon**[3,*], **Juan Oses-Prieto**[4], **Young-wook Jun**[5], **Barry S. Taylor**[2,6,7], **Alma Burlingame**[4], **Charles S. Craik**[4], and **Neil P. Shah**[1,2,7]

[1]Department of Pharmaceutical Sciences and Pharmacogenomics, University of California, San Francisco, California 94143 U.S.A

[2]Division of Hematology/Oncology, University of California, San Francisco, California 94143 U.S.A

[3]Department of Chemistry and Chemical Biology, University of California, San Francisco, California 94158 U.S.A

[4]Department of Pharmaceutical Chemistry, University of California, San Francisco, California 94158 U.S.A

[5]Department of Otolaryngology, University of California, San Francisco, California 94115 U.S.A

[6]Department of Epidemiology and Biostatistics, University of California, San Francisco, California 94158 U.S.A

[7]Helen Diller Family Comprehensive Cancer Center, University of California, San Francisco, California 94143 U.S.A

Abstract

The clinical experience with BCR-ABL tyrosine kinase inhibitors (TKIs) for the treatment of chronic myeloid leukemia (CML) provides compelling evidence for oncogene addiction. Yet, the molecular basis of oncogene addiction remains elusive. Through unbiased quantitative phosphoproteomic analyses of CML cells transiently exposed to BCR-ABL TKI, we identified persistent downregulation of growth factor receptor (GF-R) signaling pathways. We then established and validated a tissue-relevant isogenic model of BCR-ABL-mediated addiction, and found evidence for myeloid GF-R signaling pathway rewiring that profoundly and persistently dampens physiologic pathway activation. We demonstrate that eventual restoration of ligand-mediated GF-R pathway activation is insufficient to fully rescue cells from a competing apoptotic fate. In contrast to previous work with BRAFV600E in melanoma cells, feedback inhibition following BCR-ABL TKI treatment is markedly prolonged, extending beyond the time required to initiate apoptosis. Mechanistically, BCR-ABL-mediated oncogene addiction is facilitated by persistent high levels of MEK-dependent negative feedback.

Corresponding Author: Neil P. Shah, M.D., Ph.D., 513 Parnassus Avenue MSB S1471, San Francisco, CA 94143, nshah@medicine.ucsf.edu, Phone: (415) 476-3303, Fax: (415) 476-3725.
*Equal Contribution

Conflict of Interest Disclosure Statement
N.P. Shah has received funding for the conduct of clinical research from Bristol-Myers Squibb and Ariad Pharmaceuticals. N.P. Shah has served as an ad hoc consultant for Bristol-Myers Squibb and Ariad Pharmaceuticals.

Keywords

BCR-ABL; Negative Feedback; Phosphoproteomics; JAK2; Oncogene Addiction

INTRODUCTION

Translational studies with small molecule tyrosine kinase inhibitors (TKIs) in patients with chronic myeloid leukemia (CML) have convincingly demonstrated that the clinical activity of these agents is achieved through inhibition of the intended target BCR-ABL (1). To date, the high rate of success associated with BCR-ABL TKIs provides the most compelling clinical evidence for the phenomenon of "oncogene addiction", the exquisite reliance of cancer cells upon a pathologically activated oncogene. Oncogene addiction enables targeted therapies to effect clinical responses and simultaneously cause little toxicity. Even in the most advanced phases of CML, a substantial proportion of patients can achieve deep responses with BCR-ABL TKIs (2).

Our understanding of the molecular basis of oncogene addiction is poor. Sharma et al proposed the term "oncogenic shock" to describe the effect that activated oncogenes have on the balance between prosurvival and proapoptotic signals. The oncogenic shock model proposes that upon acute inhibition of oncogene activity, a more rapid decay in prosurvival signals leads to a state that favors apoptosis (3). While this model provides a useful conceptual framework in which to begin to understand the phenomenon of oncogene addiction, evidence to support the oncogenic shock model is largely circumstantial; molecular mechanisms that lead to the proposed heightened levels of prosurvival and proapoptotic signals have not been well-characterized.

Over the past decade, numerous oncogenic kinases in a variety of cancers have been identified and clinically targeted, including EGFR and ALK in non-small cell lung cancer, BRAFV600E in melanoma and colorectal cancer, and FLT3-ITD in acute myeloid leukemia (AML). However, efforts to extrapolate the clinical success of BCR-ABL TKI therapy in CML to other malignancies have failed; the majority of patients treated with other clinically active TKIs do not achieve responses of similar magnitude. For example, the selective BRAF inhibitor vemurafenib, which is approved for BRAFV600E-positive metastatic melanoma, rarely effects deep reductions in tumor volume (4). Interestingly, MEK inhibitors are active in BRAFV600E-expressing cells *in vitro* but, unexpectedly, not in cells with activated receptor tyrosine kinases (RTKs) that activate the RAS/MEK/ERK pathway (5). Previous studies demonstrated that BRAFV600E establishes a high level of ERK-directed transcriptional output and MEK-dependent negative feedback of growth factor-receptor (GF-R) signaling, whereas activated oncogenic RTKs do not. Additionally, in contrast to RTKs, BRAFV600E escapes MEK-dependent negative feedback (6).

It has been postulated that efficient bypass of BRAF kinase inhibition through GF-R-mediated re-activation of the RAS/MAPK signaling pathway may allow melanoma cells to survive in the tumor microenvironment. Recent experimental data has demonstrated that melanoma, colorectal, and thyroid cancer cells harboring BRAFV600E mutations are

inherently primed to circumvent BRAF inhibition by vemurafenib through rapid relief of negative feedback of GF-R signaling (7–11).

Here, we sought to characterize the molecular mechanisms that underlie BCR-ABL-mediated oncogene addiction in an effort to understand what makes this kinase the best-validated target in human cancer. We applied an unbiased kinetic quantitative phosphoproteomic analysis to CML cells transiently exposed to the BCR-ABL TKI dasatinib to identify candidate mediators of BCR-ABL-dependent cell survival. To test the importance of the observed signaling changes, we established a tissue and species-relevant isogenic model system to molecularly characterize BCR-ABL-mediated oncogene addiction and validated our findings in patient-derived cell lines.

RESULTS

Phosphoproteomic Analysis of Pulsed Dasatinib-Treated CML Cells Reveals Durable Alterations in Growth-Factor Signaling Pathways

Previous work demonstrated that transient exposure (20 minutes) of CML cell lines to clinically relevant concentrations of dasatinib elicits apoptosis with kinetics similar to continuous TKI exposure, despite evidence that BCR-ABL kinase activity is largely restored within four hours of drug washout (12–14). We hypothesized that the phosphorylation status of a subset of proteins must be durably altered, and critical mediators of BCR-ABL-mediated cell survival would be included amongst this group. We therefore undertook an unbiased kinetic, quantitative assessment of phosphotyrosine-containing proteins in the CML patient-derived cell line, K562, transiently exposed to a high-dose pulse (HDP) of 100nM dasatinib using stable isotope labeling by amino acids in culture (SILAC). We successfully identified 184 phosphotyrosine residues in 126 different proteins, representing the most comprehensive kinetic analysis of TKI-treated CML patient-derived cells to date (supplemental table 1). We compared the quantified phosphotyrosine profile before TKI treatment, after 20 minutes of TKI exposure, and at three and six hours after TKI washout (figure 1a).

We grouped phosphotyrosine peptides based on the pattern of tyrosine modification following HDP dasatinib treatment. Twenty-four tyrosine residues were transiently dephosphorylated, 31 were gradually dephosphorylated, 46 were not appreciably altered, and seven were hyperphosphorylated. Notably, 55 tyrosine residues were persistently dephosphorylated following TKI washout, and functional enrichment of these peptides revealed an over-representation of proteins involved in GF-R signaling pathways (supplemental table 2). Amongst these were tyrosine residues from STAT5A/B, ERK1/2, GAB1 and SHC1. Phosphotyrosine peptides associated with PI3K/AKT pathway activation were either transiently dephosphorylated or not altered (figure 1b). Several of the signaling changes identified in the phosphoproteomic analysis were confirmed by western immunoblot in K562 cells and the independent patient-derived CML cell line KU812. While tyrosine residues within the PI3K/AKT pathway were not durably altered in the phosphoproteomic analysis, serine phosphorylation of S6 (S235/S236) was durably altered in a time-dependent manner following TKI treatment (figure 1c). Similar phosphorylation changes were observed in K562 and KU812 cells treated with a HDP of the BCR-ABL TKI

imatinib (supplemental figure 1), arguing that the observed signaling changes are likely a consequence of BCR-ABL inhibition, and not the result of unintended off-target kinase inhibition.

Although phosphorylation at the BCR-ABL activation loop site Y393, which is essential for kinase activity, was only transiently absent following HDP dasatinib treatment, phosphoproteomic and western immunoblot analyses revealed substantial variation in phosphorylation changes of BCR-ABL tyrosine residues (figure 1d). Collectively, our phosphoproteomic and immunoblot analyses, coupled with previous studies, suggest a requirement for the maintenance of at least two of the three canonical BCR-ABL activated pathways (JAK/STAT, RAS/MEK/ERK, and PI3K) for CML cell survival *in vitro* (15). Furthermore, these observations suggest that persistent activation of GF-R signaling pathways is critical for BCR-ABL-mediated oncogene addiction.

BCR-ABL Confers a State of Oncogene Addiction in Human Myeloid Cells *In Vitro*

To investigate whether BCR-ABL appropriates GF-R signaling pathways to establish oncogene addiction, we sought to model oncogene addiction *in vitro* by establishing an isogenic cell line model system. Human-derived erythroleukemia TF1 cells require hGM-CSF or hIL-3 for proliferation and survival *in vitro*, but can be transformed to growth factor independence by BCR-ABL (16). We established pools of TF1/puro and TF1/BCR-ABL cells through retroviral transduction. Western immunoblot analysis confirmed the expression of phosphorylated BCR-ABL protein in TF1/BCR-ABL cells and activation of downstream targets CRKL, STAT5A/B, ERK1/2 and S6 (supplemental figure 2a, 2b).

To determine if TF1/BCR-ABL cells have acquired reliance upon BCR-ABL activity for survival and thereby truly represent a model of oncogene addiction, we measured the amount of apoptosis induced in response to simultaneous growth factor deprivation and dasatinib treatment. In TF1/puro cells hGM-CSF-deprivation alone led to decreased viability, and dasatinib had no additional impact on the extent of apoptosis induced. In sharp contrast, TF1/BCR-ABL cells underwent a statistically significant increase in apoptosis when treated with dasatinib (figure 2a). Moreover, continuous co-treatment with hGM-CSF and dasatinib fully rescued TF1/puro cells from apoptosis, while TF1/BCR-ABL cells were only partially rescued from dasatinib-mediated apoptosis by hGM-CSF. These results demonstrate that BCR-ABL establishes a state of oncogene addiction in TF1 cells, which is associated with functionally altered GM-CSF receptor (GM-CSFR) signaling. More broadly, these findings implicate rewiring of GF-R signaling pathways in the establishment of the BCR-ABL-addicted state.

BCR-ABL Kinase Activity Attenuates GM-CSFR Signal Transduction in TF1 Cells

To further characterize the GM-CSFR signaling axis and to investigate the molecular mechanisms through which BCR-ABL may subvert GF-R signaling, we cultured TF1/puro and TF1/BCR-ABL cells under serum and growth factor-deprived conditions and then stimulated the cells with hGM-CSF, which activates the JAK2/STAT5, RAS/MAPK, and PI3K/AKT signaling pathways (17). While robust activation of JAK2 was observed in both cell lines, GTP loading of RAS was only observed in hGM-CSF-stimulated TF1/puro cells

(figure 2b; lanes 3 versus lanes 7 and supplemental figure 2c, 2d). We also assessed the effect of a one-hour dasatinib pretreatment prior to stimulation with hGM-CSF. Again, increased RAS-GTP loading was only observed in TF1/puro cells (figure 2b; lane 4 versus lane 8 and supplemental figure 2c, 2d) and hGM-CSF-mediated STAT5, ERK, and AKT activation was substantially attenuated in TF1/BCR-ABL cells relative to TF1/puro cells. Collectively, these data demonstrate that BCR-ABL kinase activity negatively regulates GM-CSFR signaling, and this regulation persists for more than one hour following BCR-ABL kinase inhibition.

To determine if GF-R signaling in BCR-ABL-expressing cells can be fully restored within 2–4 hours following kinase inhibition, as has been observed with vemurafenib-treated BRAFV600E melanoma cells stimulated with HGF, EGF, or NRG1 (7, 9, 10), TF1/puro and TF1/BCR-ABL cells were treated with BCR-ABL TKI for up to eight hours prior to hGM-CSF stimulation. While a gradual increase in the hGM-CSF-mediated activation of STAT5, ERK, and AKT was observed with more prolonged BCR-ABL inhibition (figure 2c; lanes 9, 10, 11, 12), the magnitude of pathway reactivation in TF1/BCR-ABL cells after eight hours of BCR-ABL kinase inhibition was substantially less than that observed in TF1/puro cells (figure 2c; lanes 3, 4, 5, 6). Additionally, despite moderate hGM-CSF-mediated rephosphorylation of ERK in TF1/BCR-ABL cells after eight hours of BCR-ABL inhibition, RAS activation was minimal. BCR-ABL inhibition was maintained throughout this period, as evidenced by dephosphorylation of the activation loop tyrosine Y393 (figure 2c; lanes 9, 10, 11, 12).

We next assessed whether more prolonged BCR-ABL inhibition is required to enable a near complete restoration of GM-CSFR signaling. Indeed, treatment of TF1/puro and TF1/BCR-ABL cells with dasatinib for 24 hours prior to hGM-CSF stimulation resulted in more complete RAS activation in TF1/BCR-ABL cells (figure 2d). Similarly, activation of STAT5, ERK, and AKT was restored to levels comparable to those observed in TF1/puro cells (figure 2e). However, as demonstrated earlier, despite this delayed restoration of growth factor signaling, hGM-CSF failed to fully rescue TF1/BCR-ABL cells from TKI-mediated apoptosis (figure 2a). These results demonstrate an important biologic consequence of GF-R signaling rewiring by BCR-ABL: a substantial proportion of cells commit to apoptosis despite the eventual reestablishment of prosurvival growth factor signaling. Similar results were obtained when TF1/puro and TF1/BCR-ABL cells were treated with imatinib, indicating these effects are due to inhibition of BCR-ABL and not other targets of the TKI (supplemental figure 3a–3d).

BCR-ABL Kinase Activity Attenuates Erythropoietin Receptor Signal Transduction in CML Patient-derived Cells

To extend our findings to a CML patient-derived cell line, we evaluated whether BCR-ABL rewires GF-R signaling in K562 cells, which express a functional erythropoietin receptor (EPO-R) (18). Relative to HEL erythroleukemia cells harboring the activating JAK2/V617F allele, K562 cells exhibit nearly undetectable levels of JAK2 Y1007 phosphorylation in the absence of erythropoietin (hEPO) (supplemental figure 4a). Stimulation of K562 cells with hEPO led to a modest increase in JAK2 activation; one hour pretreatment with a BCR-ABL

TKI prior to hEPO stimulation did not appreciably impact the degree of JAK2 activation (figure 3a).

We next assessed the effect of prolonged BCR-ABL inhibition (2–24 hours) on hEPO-mediated activation of JAK2 and downstream pathways in K562 cells. A time-dependent increase in hEPO-mediated STAT5, ERK and AKT activation occurred with either dasatinib or imatinib pre-treatment (figure 3b and supplemental figure 4b). A statistically significant increase in the degree of hEPO-mediated activation of JAK2 (figure 3c and supplemental figure 4c) and a substantial increase in RAS activity (figure 3d) were observed following 24 hours BCR-ABL TKI pre-treatment.

JAK2 Activity Becomes Critical for EPO-R Signaling and K562 Cell Survival After Prolonged BCR-ABL Inhibition

To determine if restoration of EPO-R signaling following prolonged BCR-ABL inhibition is mediated through the canonical EPO-R/JAK2 axis, we utilized the selective JAK2 inhibitor TG101348. Combined 24 hour pre-treatment of K562 cells with TG101348 and a BCR-ABL TKI completely prevented hEPO-mediated JAK2 activation and re-phosphorylation of STAT5, ERK, and AKT (figure 3e and figure 3f, **lanes 8,9, 11 and 12**). Similar to the partial rescue from apoptosis hGM-CSF provides TKI-treated TF1/BCR-ABL cells (figure 2a), hEPO partially rescues K562 cells from imatinib-mediated apoptosis [(19) and supplemental table 3]. This partial rescue from imatinib (or dasatinib)-mediated apoptosis was completely reversed by co-administration of TG101348. However, in the setting of active BCR-ABL, TG101348 had no pro-apoptotic effect on K562 cells (supplemental table 3). These observations suggest that JAK2 kinase is minimally active in the presence of BCR-ABL kinase activity, but can become critical for growth-factor-mediated CML cell survival upon prolonged BCR-ABL inhibition.

BCR-ABL Inhibition Down-regulates Modulators of Negative Feedback and Upregulates EPO-R

To better understand the mechanism(s) responsible for the inability of GF-Rs to effectively transduce signal in BCR-ABL-expressing cells, time-dependent changes in global gene expression were assessed in K562 cells were treated with dasatinib. In total, microarray analysis revealed 1903 genes that were significantly differentially expressed at either four, eight, or 24 hours of dasatinib treatment (supplemental table 4). As negative regulators of RAS/MAPK signaling were previously shown to be down-regulated early after MAPK inhibition in BRAFV600E cells (6), we reasoned that key negative regulators of EPO-R signaling in K562 cells would be enriched among genes significantly down-regulated after four hours of dasatinib treatment. In total, 162 genes followed this pattern (FDR<1%) including well-characterized members of the JAK/STAT and RAS/MAPK negative feedback machinery: *SOCS1*, *SOCS2*, *CISH*, *SPRY2*, *SPRY4*, *SPRED1*, *SPRED2*, and *PIM1*, but notably excluded were others such as *DUSP4* and *DUSP6* (figure 4a). Other genes among these 162 potently down-regulated after four hours of treatment were downstream effectors of MEK/ERK signaling, such as cyclin D1 (*CCND1*) as well as genes that traditionally comprise ERK-mediated transcriptional output including transcription factors

associated with transformation (*ETV5* and *MYC*) among other ERK targets (*IER3* and *EGR1*).

We explored the 1048 unique probes whose expression increased following dasatinib treatment to identify genes that become de-repressed following prolonged BCR-ABL inhibition, as might be expected of positive effectors of GF-R signaling, such as JAK2 or the SRC family kinases. Several non-canonical dual-specificity phosphatases (DUSPs) not traditionally involved in negative feedback regulation of the RAS pathway were among this group of genes (i.e. DUSP1, DUSP13, DUSP21, DUSP28). Interestingly, EPO-R expression increased significantly in a time-dependent manner in dasatinib-treated cells. The observed changes in a subset of these genes were validated by quantitative PCR (qPCR) in dasatinib and imatinib treated K562 cells (figure 4b). Similar changes in gene expression were observed in K562 cells treated with the MEK inhibitor PD0325901, suggesting that the RAS/MAPK pathway is primarily responsible for establishing the negative feedback network and transcriptional output associated with attenuation of myeloid GF-R signaling.

MEK/ERK-Dependent Negative Feedback Attenuates EPO-R Signaling in K562 Cells

To assess the functional importance of MEK-dependent negative feedback toward GF-R signaling attenuation in CML cells, we treated K562 cells with PD0325901 for 24 hours. MEK inhibition alone (in the absence of hEPO stimulation) produced robust GTP-loading of RAS (figure 4c; lane 3), whereas co-treatment with dasatinib and PD0325901 prevented RAS GTP-loading, demonstrating that RAS activation upon MEK inhibition is mediated by BCR-ABL and is not the result of exogenous or autocrine growth factors (figure 4c; lane 3 and 4), as has been recently documented to occur in AML, where HGF secretion by leukemic cells can foster survival in the setting of kinase inhibitor treatment (20). hEPO stimulation of PD0325901 pre-treated cells resulted in further RAS activation, demonstrating that efficient EPO-R signaling in K562 cells can be restored by MEK inhibition alone (figure 4c; lane 3 and lane 7 and supplemental figure 5a).

To investigate whether MEK-dependent negative feedback dampens EPO-R signaling at the level of JAK2, we assessed JAK2 phosphorylation in response to hEPO after a 24-hour pretreatment with PD0325901. hEPO-mediated JAK2 activation was comparable to that observed with a 24-hour dasatinib pretreatment (figure 4d; supplemental figure 5b), demonstrating that MEK-dependent negative feedback acts at the level of EPO-R/JAK2 in K562 cells. No further increase in hEPO-mediated JAK2 activation was detected when cells were pretreated with the combination of dasatinib and MEK inhibitor for 24 hours prior to hEPO stimulation (figure 4d; lanes 6, 7 versus lane 8). In the absence of hEPO stimulation, MEK inhibition did not result in a detectable increase in JAK2 phosphorylation (figure 4d; lane 3).

To determine if BCR-ABL is itself subjected to MEK-dependent negative feedback, we evaluated the effect of MEK inhibition upon the phosphorylation status of multiple BCR-ABL tyrosine residues, including the activation loop tyrosine (Y393). Across all BCR-ABL phosphotyrosine residues interrogated, little to no change in phosphorylation was observed (supplemental figure 5c), suggesting that similar to BRAFV600E and in sharp contrast to

RTKs (6), BCR-ABL both establishes and evades a high level of MEK-dependent negative feedback regulation.

K562 Cells Can Commit to Apoptosis Prior to Full Restoration of EPO-R Signaling

The long delay observed in the restoration of EPO-mediated pathway activation in K562 cells sharply contrasts with the rapid (~2–4 hours) and full reactivation of the MEK/ERK pathway in EGF-stimulated BRAFV600E cells following pre-treatment with vemurafenib (10). This finding, coupled with the inability of hEPO to fully rescue K562 cells from dasatinib-mediated apoptosis, suggests that TKI-treated CML cells face competing fates: growth factor-mediated survival versus commitment to apoptosis prior to complete restoration of GF-R signaling. To formally test this, we initially assessed the kinetics of apoptosis induction in TKI-treated K562 cells by western immunoblot. While substantial caspase-3 cleavage was detected after 24 hours of dasatinib treatment, we observed very little evidence of apoptosis following 12 hours of treatment (figure 5a). To detect caspase-3 activity with a higher degree of sensitivity, we employed a plasmonic nanosensor technique capable of detecting single molecule caspase-3 cleavage events through a change in light scattering intensity of a gold nanoshell pair (figure 5b; 5c) (21). This assay reliably detected caspase-3 activity following only eight hours of dasatinib treatment (figure 5d), demonstrating that a commitment to apoptosis can precede full restoration of GF-R signaling in CML patient-derived BCR-ABL-addicted cells.

BCR-ABL-Dependent Negative Feedback Differs from BRAFV600E and Oncogenic Myeloid RTK-Mediated Negative Feedback in TF1 Cells

Although both the quality and quantity of negative feedback following inhibition of BRAFV600E in melanoma and thyroid cancer cell lines appear to differ from inhibition of BCR-ABL in CML cells (10, 11), we sought to directly compare the molecular mediators and duration of negative feedback induced by BCR-ABL, BRAFV600E and an oncogenic RTK in the same cellular context. We therefore introduced BRAFV600E, FLT3-ITD, FLT3-D835V and BCR-ABL into TF1 cells. While hGM-CSF-independent TF1 populations expressing BCR-ABL, FLT3-ITD and FLT3-D835V were readily established, multiple attempts to obtain a factor-independent pool of BRAFV600E-expressing TF1 cells failed. We carefully studied the immediate fate of TF1 cells infected with MIG-BRAFV600E, MIG-BCR-ABL, MIG-FLT3-ITD and MIG-FLT3-D835V. Following transduction, infected cells were sorted and their growth in hGM-CSF was monitored. TF1/MIG-BCR-ABL, TF1/MIG-FLT3-ITD, and TF1/MIG-FLT3-D835V cells grew somewhat more slowly than control TF1/MIG cells, suggesting that both BCR-ABL- and oncogenic FLT3-dependent negative feedback partially dampen hGM-CSF responsiveness (figure 6a). Interestingly, the growth rate of TF1/BCR-ABL was significantly slower than that of TF1/FLT3-ITD and TF1/FLT3-D835V, suggesting that negative feedback elicited by BCR-ABL differs in magnitude from that elicited by oncogenic FLT3. In contrast, the growth of TF1/BRAFV600E was significantly attenuated relative to all other cell lines despite the presence of hGM-CSF, suggesting that expression of BRAFV600E profoundly diminishes hGM-CSF responsiveness. Indeed, high levels of ERK1/2 activation were observed in TF1/MIG-BRAFV600E cells after transduction, and although we eventually observed hGM-CSF-supported growth of these cells, ERK1/2 activation was substantially diminished when this

occurred (supplemental figure 6). This observation suggests that compensation for BRAFV600E signaling through attenuation of BRAFV600E-directed negative feedback may be necessary for growth factor-mediated proliferation of TF1/BRAFV600E cells.

To test if the molecular mediators of negative feedback elicited by an oncogenic RTK differ from BCR-ABL, we first assessed the state of oncogene addiction mediated by FLT3-ITD expression in TF1 cells. Similar to TF1/BCR-ABL cells treated with BCR-ABL TKI, growth factor-deprived TF1/FLT3-ITD cells are significantly more sensitive to treatment with the potent selective FLT3 inhibitor AC220 (quizartinib) when compared with growth factor-deprived TF1/puro cells (figure 6b). However, in contrast to what we previously observed with TF1/BCR-ABL cells, hGM-CSF more fully rescued TF1/FLT3-ITD cells from AC220-mediated apoptosis. To assess whether the duration of negative feedback in TF1/FLT3-ITD cells following kinase inhibition differs from what we observed in TF1/BCR-ABL cells, we treated TF1/FLT3-ITD cells with AC220 for varying lengths of time prior to hGM-CSF stimulation. In contrast to TF1/BCR-ABL cells, hGM-CSF-mediated activation of STAT5A/B and ERK1/2 was fully restored following only two hours of kinase inhibition (figure 6c), suggesting that, similar to what is observed following BRAFV600E inhibitor treatment in melanoma and thyroid cancer cell lines, FLT3-ITD-dependent negative feedback rapidly diminishes following FLT3-inhibition. Interestingly, the kinetics of GM-CSFR-mediated AKT phosphorylation following kinase inhibitor treatment differs between TF1/BCR-ABL and TF1/FLT3-ITD cells. In TF1/BCR-ABL cells, partial AKT rephosphorylation was observed after 2–4 hours of dasatinib treatment (figure 2c) while prolonged FLT3-ITD inhibition was necessary for GM-CSFR-mediated AKT phosphorylation in TF1/FLT3-ITD cells. These results highlight the substantial differences in negative feedback elicited by BCR-ABL and an oncogenic RTK.

DISCUSSION

The efficacy of BCR-ABL TKI therapy for CML surpasses that of all other FDA-approved targeted kinase inhibitors and thereby provides the most compelling clinical example of oncogene addiction. Our poor understanding of the molecular basis of this phenomenon has been due, in part, to a lack of effective models. Here, we transiently exposed CML cells to dasatinib and identified durable changes in effectors of GF-R signaling, which likely explain the cytotoxic effects of BCR-ABL inhibition. We then established and validated an isogenic system of BCR-ABL-mediated oncogene addiction and investigated its molecular features. We found that BCR-ABL-mediated oncogene addiction is the result of physiologic negative feedback inhibition that functionally and persistently dampens GF-R signaling at multiple nodes, including, in the case of EPO-R, at the level of GF-R transcription. As with BRAFV600E in melanoma cells, BCR-ABL establishes a high level of MEK-dependent negative feedback. Relief from MEK-dependent negative feedback is required to enable full restoration of GF-R signaling and only occurs after prolonged BCR-ABL kinase inhibition. Importantly, negative feedback dampens GF-R signaling substantially longer in CML cells than what has been reported in BRAFV600E-expressing melanoma cells. As a consequence, GF-R signaling is insufficient to fully rescue CML cells from the competing fate of apoptosis, which for the first time, we demonstrate to be initiated as early as eight hours following TKI treatment. As a result of this interplay between a commitment to apoptosis

and the decay of negative feedback that facilitates restoration of prosurvival growth factor signaling, CML cells demonstrate a profound reliance upon BCR-ABL kinase activity for survival (figure 7a; 7b).

Both experimental and clinical evidence suggest that the effectiveness of BRAFV600E inhibition in melanoma contrasts sharply with BCR-ABL inhibition in CML. *In vitro*, BRAFV600E melanoma cell lines largely fail to undergo apoptosis when treated with BRAF inhibitors such as vemurafenib (22–25) and although the majority of melanoma patients treated with vemurafinib respond to some degree, most fail to achieve deep remissions (4). A number of BRAFV600E-expressing melanoma, colorectal, and thyroid cancer cell lines can be rescued from BRAF inhibitor treatment by RTK ligands *in vitro*, leading to subsequent reactivation of MAPK and AKT signaling as soon as one hour after BRAF inhibitor treatment (7–11). In contrast, the corresponding time frame we observed in BCR-ABL-expressing cells is markedly different: only partial restoration of GF-R signaling occurs after eight hours of TKI treatment, at which time a competing commitment to apoptosis has already been initiated in a substantial proportion of cells.

Despite the clinical differences observed with inhibitors of BRAFV600E and BCR-ABL, these two oncoproteins share some biological properties. Both are pathologically activated cytosolic kinases that establish and evade a high-degree of MEK-dependent negative feedback (6). Also, a substantial core component of the ERK transcriptional output is similarly diminished when these oncoproteins are inhibited, including ERK pathway effectors, negative feedback regulators, and downstream transcription factors. For instance, both kinases appear to induce the expression of members of the Sprouty gene family, which typically target the ERK pathway for negative feedback inhibition at the level of RAF, RAS and upstream RTKs.

There are, however, notable differences in the negative feedback networks generated by BCR-ABL and BRAFV600E, particularly with respect to where feedback is operable. At the GF-R level, BCR-ABL kinase activity down-regulates EPO-R expression in K562 cells, largely through MEK/ERK signaling, which may further contribute to the delay in restoring pro-survival GF-R-mediated signaling following BCR-ABL inhibition. In contrast, experimental evidence suggests that there is sufficient RTK expression in BRAFV600E melanoma and colorectal cancer cells to rapidly restore pro-survival signaling (7–10). Additional differences exist in downstream components of negative feedback, particularly at the level of ERK phosphatases, which target either nuclear or cytosolic ERK for regulation downstream of the oncogenic insult. In sharp contrast to the effect of BRAFV600E inhibition in melanoma cells where downregulation of the dual specificity phosphatase DUSP6 is apparent at multiple levels (6, 10), we failed to detect DUSP6 at the protein level in CML cells (data not shown) and, in agreement with this observation, BCR-ABL inhibition failed to down-regulate *DUSP6* expression. These differences suggest that MEK-dependent negative feedback is oncogene-specific. Moreover, in BCR-ABL-expressing CML cells, feedback effectors of the parallel JAK/STAT pathway are activated (e.g. *SOCS1* and *SOCS2*), while in BRAFV600E melanoma cells these feedback effectors are absent. These results reaffirm that the networks mediating negative feedback inhibition of oncogenic signaling are multifaceted, pleiotropic, and context-dependent. Indeed, expression

of oncogenic alleles of FLT3 in TF1 cells demonstrates that activation of a clinically relevant myeloid RTK elicits a negative feedback response that is clearly distinct from that elicited by BCR-ABL in the same cellular context. Further study is required to dissect the importance of the observed qualitative and quantitative differences in negative feedback elicited by these kinases.

Our work provides insight into the role of JAK2 in the molecular pathogenesis of CML, which has been a subject of considerable controversy. It is known that CML stem cells persist for at least several years in most, if not all, CML patients. It has been speculated that successful inhibition of BCR-ABL kinase activity in CML stem cells may be insufficient to elicit apoptosis in these cells due to their residence in a cytokine-rich bone marrow microenvironment that maintains their viability despite BCR-ABL TKI treatment (26). One group provided evidence that combined BCR-ABL and JAK2 inhibition achieves more complete eradication of CML cells in conditioned media *in vitro* (27), while another group recently demonstrated that JAK2 is completely dispensable for nearly all aspects of BCR-ABL-mediated myeloid disease initiation and maintenance (28). Although these studies offer conflicting views on the importance of JAK2 activity for CML pathogenesis, our results and proposed model of BCR-ABL-dependent attenuation of GF-R signaling resolves this apparent paradox. When BCR-ABL is active, JAK2 plays little or no role in signal transduction due to MEK-dependent negative feedback-mediated attenuation of GF-R signaling. After prolonged BCR-ABL inhibition, negative feedback is relieved and JAK2 may become critically important as a mediator of STAT5 phosphorylation in the setting of external growth factors. Our data provide mechanistic support for clinical efforts to combine BCR-ABL TKIs with potent JAK2 TKIs, which are predicted to have no activity in the absence of BCR-ABL inhibition, but might demonstrate a synthetic lethal interaction with BCR-ABL TKIs in the setting of exogenous growth factors, specifically as a consequence of the decay in negative feedback we describe here. If JAK2 serves a redundant function in facilitating prosurvival GF-R mediated signaling in the bone marrow microenvironment, alternative approaches will be required.

The oncogenic shock model of oncogene addiction (3) was proposed with limited supporting data, and the molecular mediators of oncogene addiction have remained elusive. Our data strongly implicate persistent negative feedback in the promotion of apoptosis following kinase inactivation, and thus provide valuable molecular mechanistic insights into the basis of both oncogene addiction and the oncogenic shock model. The recent appreciation of how rapidly negative feedback decays in BRAFV600E-expressing systems and thereby facilitates prosurvival signal transduction by GF-Rs has led to treatment approaches that combine vemurafenib with multikinase GF-R inhibitors. However, given the growing number of signaling molecules that have been found to become activated following inhibition of BRAFV600E, safe and effective inhibition of all relevant GF-Rs may prove difficult. Our studies of BCR-ABL-mediated oncogene addiction suggest an alternative approach aimed at potentiating negative feedback in the setting of inhibition of pathologically-activated kinases, which is predicted to enhance oncogene addiction and increase sensitivity to targeted therapy. In addition to possibly facilitating deeper clinical responses, this strategy may be applicable to a broad range of malignancies associated with activating mutations in

actionable signaling molecules. Efforts to further dissect and modulate molecular mechanisms of negative feedback in relevant tissue contexts are required to formally test this prediction.

EXPERIMENTAL PROCEDURES

Cell Line Propagation and Isogenic Cell Line Generation

Cell lines were propagated in RPMI 1640 medium supplemented with 10% fetal bovine serum (FBS; Omega Scientific), L-glutamine, and penicillin/streptomycin (Invitrogen). K562 and KU812 cells were purchased from American Type Culture Collection (ATCC). TF1 cells were a kind gift from Michael Tomasson (Washington University, St. Louis, MO). All cell lines were authenticated by Promega STR analysis. To generate isogenic cell lines, TF1 cells were engineered to express the ecotropic-receptor (Eco-R) through retroviral transduction (pMOWS-EcoR plasmid) as previously described (29). TF1-Eco-R cells underwent a second round of retroviral transduction with pMSCV-puro, pMSCV-BCR-ABL and puromycin selection. TF1/BCR-ABL cells were selected for growth-factor independence while TF1/puro cells were supplemented with 2ng/mL hGM-CSF (Peprotech) under normal growth conditions.

Kinase Inhibitors and Drug Treatments

Imatinib and dasatinib were purified at UCSF. TG101348, PD0325901, and AC220 were purchased from Selleckchem. All drug exposures were performed at a density of 5×10^6 cells/mL. For cytokine stimulation, cells were starved in 0.1% FBS-RPMI as indicated and subsequently stimulated with 1U/mL human erythropoietin (hEPO) (R&D Systems) or 10ng/mL of hGM-CSF. Dasatinib HDP and LDC drug exposures were performed as described previously (12).

Statistical Analyses

All statistical analyses were performed in Prism (GraphPad) using a two-way ANOVA with Bonferroni post-tests.

Quantitative Phosphoproteomics and DAVID Functional Analysis

K562 cells were grown for six days in customized RPMI 1640 supplemented with heavy (Cambridge Isotope Laboratories; CLM-2265 and CLM-2247) or light (Sigma-Aldrich) 30mg/L Arginine, 40mg/L Lysine, and 10% dialyzed FBS (Invitrogen) prior to drug treatment. The PY100 Phosphoscan Kit (Cell Signaling Technology) was used to enrich phosphotyrosine containing tryptic peptides. To reduce sample complexity prior to MS/MS analysis, phosphotyrosine peptides were fractionated step-wise under alkaline conditions (20mM ammonium formiate, pH 10.3) with increasing amounts of acetonitrile (5% ACN, 10% ACN, 15% ACN, 20% ACN, 90% ACN). Peptides were separated and analyzed using a nano-LC column coupled to a LTQ OrbiTrap XL (Thermo Scientific) at the UCSF Mass Spectrometry Core Facility. An in-house software analysis program was used to extract quantitative information for all identified peptides from each nano-LC analysis for all time points. Heat map representation of the phosphoproteomic data was generated using GENE-E (http://www.broadinstitute.org/cancer/software/GENE-E/). We functionally characterized

phosphosites durably altered by HDP dasatinib treatment relative to all identified phosphoproteins (background) using the DAVID tool with default parameters (30, 31)

Cell Lysis and Protein Immunoprecipitation

Cells were lysed in JAK2 IP buffer (50mM Tris pH 7.6, 100mM NaCl, 1mM EDTA, 1mM EGTA, 0.5% NP40, 0.1% Triton) or RAS IP buffer (50mM Tris pH 7.5, 125mM NaCl, 6.5mM $MgCl_2$, 5% glycerol, 0.2% NP40) supplemented with 1% protease and 1% phosphatase inhibitors (Calbiochem). For JAK2 immunoprecipitations, normalized lysates were tumbled overnight at 4°C with anti-total JAK2 antibody (1:100) (Cell Signaling Technology, cat. #3230). Immunoprecipitated JAK2 was collected with protein A Dynabeads (Invitrogen). For RAS GTP-pulldown assays, normalized lysates were tumbled for 1hr at 4°C with 20μL of RAS Assay Reagent (Millipore; #14-278).

Antibodies, Western Immunoblot, and Phospho-Flow Cytometry

Cell lysates were resolved by SDS-PAGE and transferred to nitrocellulose as described previously (12). Phospho- and total antibodies for STAT5A/B (phospho-Y694/Y699) (cat. 9351 and 9363), ERK1/2(phospho-T202/Y204)(cat. 4370 and 9107), AKT (phospho-S473) (cat. 4060 and 9272), S6 (phospho-S235/S236) (cat. 2211 and 2317), CRKL (phospho-Y207) (cat. 3181), JAK2 (phospho-Y1007) (cat. 3776 and 3230), BCR (phospho-Y177) (cat. 3901), cABL (phospho-Y245 and phospho-Y204) (cat. 2861 and 3009), and cleaved CASP3 (cat. 9664) were purchased from Cell Signaling Technology. cABL (cat. OP20) and total RAS (cat. 05-516) antibodies were purchased from Millipore. cABL (phospho-Y134) (cat. AP3011a) and cABL (phospho-Y251) (cat. AP3014a) antibodies were purchased from Abgent. Total GAPDH (cat. sc-25778) was purchased from Santa Cruz. Odyssey infrared imaging technology and software (LI-COR Biosciences) was used for western immunoblot visualization and quantitation was measured by pixel integrated intensity. Cleaved caspase-3 was measured by flow cytometry using FITC-conjugated anti-active caspase-3 antibody (BD; cat. #550480). Analysis of CRKL phosphorylation by flow cytometry was performed as previously reported (12).

Gene Expression Analysis and Quantitative PCR

Total cellular RNA was extracted utilizing the Qiagen RNeasy kit. For Illumina gene expression analysis, RNA integrity was assessed on a Bioanalyzer using the Agilent RNA 6000 Nano Kit (5067-1511), and cRNA was generated by Ambion Illumina TotalPrep RNA Amplification kit (AMIL1791). SuperScriptII (Invitrogen) was used to generate cDNA from 2μg of extracted total cellular RNA. Samples were hybridized to the Illumina HT-12 platform by the UCSF Genomics Core and both raw control and sample probe intensities were converted to expression estimates after adjusting for array background, variance stabilization, and normalization, all with the lumi pipeline (PMID: 18467348). Differential gene expression was assessed as a time course with a two-step regression strategy (combining least-squares and stepwise regression) to identify genes with significant temporal expression changes between experimental groups (PMID: 16481333). Genes were considered significantly differentially expressed if they arose at a false discovery rate less than 1% (q-value < 0.01). Confirmatory qPCR analysis was performed using TaqMan probes and TaqMan Universal Master Mix II (Invitrogen): GAPDH (Hs02758991_g1),

SOCS1 (Hs00705164_s1), GRB10 (Hs01065498_m1), SPRY4 (Hs01935412_s1), EPOR (Hs00959427_m1). Expression array data generated in this study were deposited in the National Institutes of Health (NIH) NCBI Gene Expression Omnibus (GEO), accession number: GSE51083 (http://www.ncbi.nlm.nih.gov/geo/query/acc.cgi?acc=GSE51083).

Single Molecule Imaging of Caspase-3 Activation Using Dimeric Au Nanoshells

Techniques were adapted from (21) and modified in unpublished methods (C. Tajon, Y. Jun, and C. S. Craik). Briefly, a pair of magnetoplasmonic $Zn_{0.4}Fe_{2.6}O_4$@SiO_2@ gold (Au) nanoshells (50 nm) linked by a pegylated-peptide bearing a selective caspase-3 cleavage site were synthesized. Lysates were prepared from K562 cells pretreated for eight hours with DMSO or dasatinib, and introduced to nanosensors immobilized on a glass flow chamber. As a control 100 uM zDEVD-cmk was added for three hours. Imaging was performed on an inverted microscope (Nikon Ti-E) outfitted with a darkfield dry condenser and recorded at a temporal resolution of 10 Hz using an EMCCD detector (Andor iXon; 512×512 pixel chip). Intensity trajectories of each nanoparticle pair (n= 75) were analyzed by ImageJ. Total cleavage events observed 90 minutes following lysate introduction were counted, normalized against control, and plotted.

TF1/MIG Cell Line Growth Assay

TF-1 EcoR-expressing cells were retrovirally transduced to express MIG- BCR-ABL, FLT3-ITD, FLT3-D835V, or BRAFV600E as described above. 48 hours post-infection, GFP+ cells were sorted on a BD FACSARIA II (BD) and equivalent cell numbers were plated in 10% RPMI supplemented with 2ng/mL hGM-CSF. Cells were counted as indicated in triplicate by trypan blue exclusion. The medium and hGM-CSF was replaced as necessary and cell populations were maintained in an exponential growth phase. GFP-positivity and phospho-ERK were monitored daily by flow cytometry. Growth curves were generated by multiplying the cell count by percent GFP-positivity.

Supplementary Material

Refer to Web version on PubMed Central for supplementary material.

Acknowledgments

Financial Support: J.A. received support from the UC Cancer Research Coordinating Committee (CRCC) Fellowship and from the National Institutes of Health Training Grant T32 GM007175. Mass spectrometry analysis was provided by the Bio-Organic Biomedical Mass Spectrometry Resource at UCSF (A.L. Burlingame, Director) supported by funding from the Biomedical Technology Research Centers program of the NIH National Institute of General Medical Sciences, NIH NIGMS 8P41GM103481. E.A.L. was supported by NIH National Cancer Institute T32CA108462-07. N.P.S. is a Leukemia & Lymphoma Scholar in Clinical Research, and wishes to acknowledge the generous support of Arthur Kern, Bob Bonstein, Mark Maymar and the Edward S. Ageno family. Y. J. was supported from the National Institute of Biomedical Imaging and Bioengineering and National Institutes of Health (NIH 1R21EB015088). C.S.C received support from the National Institutes of Health (NIH R01CA128765). C.T. was supported by the UCSF Quantitative Biosciences Consortium (QBC) Fellowship and NIGMS-IMSD award (R25-GM56847). We thank Kevin Shannon and Benjamin Braun for insightful discussions.

References

1. Gorre ME, Mohammed M, Ellwood K, Hsu N, Paquette R, Rao PN, et al. Clinical resistance to STI-571 cancer therapy caused by BCR-ABL gene mutation or amplification. Science. 2001; 293:876–80. [PubMed: 11423618]
2. Druker BJ, Sawyers CL, Kantarjian H, Resta DJ, Reese SF, Ford JM, et al. Activity of a specific inhibitor of the BCR-ABL tyrosine kinase in the blast crisis of chronic myeloid leukemia and acute lymphoblastic leukemia with the Philadelphia chromosome. N Engl J Med. 2001; 344:1038–42. [PubMed: 11287973]
3. Sharma SV, Gajowniczek P, Way IP, Lee DY, Jiang J, Yuza Y, et al. A common signaling cascade may underlie “addiction” to the Src, BCR-ABL, and EGF receptor oncogenes. Cancer Cell. 2006; 10:425–35. [PubMed: 17097564]
4. Flaherty KT, Puzanov I, Kim KB, Ribas A, McArthur GA, Sosman JA, et al. Inhibition of mutated, activated BRAF in metastatic melanoma. N Engl J Med. 363:809–19. [PubMed: 20818844]
5. Solit DB, Garraway LA, Pratilas CA, Sawai A, Getz G, Basso A, et al. BRAF mutation predicts sensitivity to MEK inhibition. Nature. 2006; 439:358–62. [PubMed: 16273091]
6. Pratilas CA, Taylor BS, Ye Q, Viale A, Sander C, Solit DB, et al. (V600E)BRAF is associated with disabled feedback inhibition of RAF-MEK signaling and elevated transcriptional output of the pathway. Proc Natl Acad Sci U S A. 2009; 106:4519–24. [PubMed: 19251651]
7. Straussman R, Morikawa T, Shee K, Barzily-Rokni M, Qian ZR, Du J, et al. Tumour micro-environment elicits innate resistance to RAF inhibitors through HGF secretion. Nature. 487:500–4. [PubMed: 22763439]
8. Prahallad A, Sun C, Huang S, Di Nicolantonio F, Salazar R, Zecchin D, et al. Unresponsiveness of colon cancer to BRAF(V600E) inhibition through feedback activation of EGFR. Nature. 483:100–3. [PubMed: 22281684]
9. Wilson TR, Fridlyand J, Yan Y, Penuel E, Burton L, Chan E, et al. Widespread potential for growth-factor-driven resistance to anticancer kinase inhibitors. Nature. 487:505–9. [PubMed: 22763448]
10. Lito P, Pratilas CA, Joseph EW, Tadi M, Halilovic E, Zubrowski M, et al. Relief of profound feedback inhibition of mitogenic signaling by RAF inhibitors attenuates their activity in BRAFV600E melanomas. Cancer Cell. 22:668–82. [PubMed: 23153539]
11. Montero-Conde C, Ruiz-Llorente S, Dominguez JM, Knauf JA, Viale A, Sherman EJ, et al. Relief of feedback inhibition of HER3 transcription by RAF and MEK inhibitors attenuates their antitumor effects in BRAF-mutant thyroid carcinomas. Cancer Discov. 2013; 3:520–33. [PubMed: 23365119]
12. Shah NP, Kasap C, Weier C, Balbas M, Nicoll JM, Bleickardt E, et al. Transient potent BCR-ABL inhibition is sufficient to commit chronic myeloid leukemia cells irreversibly to apoptosis. Cancer Cell. 2008; 14:485–93. [PubMed: 19061839]
13. Hiwase DK, White DL, Powell JA, Saunders VA, Zrim SA, Frede AK, et al. Blocking cytokine signaling along with intense Bcr-Abl kinase inhibition induces apoptosis in primary CML progenitors. Leukemia. 24:771–8. [PubMed: 20130598]
14. Snead JL, O’Hare T, Adrian LT, Eide CA, Lange T, Druker BJ, et al. Acute dasatinib exposure commits Bcr-Abl-dependent cells to apoptosis. Blood. 2009; 114:3459–63. [PubMed: 19706883]
15. Sonoyama J, Matsumura I, Ezoe S, Satoh Y, Zhang X, Kataoka Y, et al. Functional cooperation among Ras, STAT5, and phosphatidylinositol 3-kinase is required for full oncogenic activities of BCR/ABL in K562 cells. J Biol Chem. 2002; 277:8076–82. [PubMed: 11779872]
16. Kitamura T, Tange T, Terasawa T, Chiba S, Kuwaki T, Miyagawa K, et al. Establishment and characterization of a unique human cell line that proliferates dependently on GM-CSF, IL-3, or erythropoietin. J Cell Physiol. 1989; 140:323–34. [PubMed: 2663885]
17. Guthridge MA, Stomski FC, Thomas D, Woodcock JM, Bagley CJ, Berndt MC, et al. Mechanism of activation of the GM-CSF, IL-3, and IL-5 family of receptors. Stem Cells. 1998; 16:301–13. [PubMed: 9766809]
18. Fraser JK, Lin FK, Berridge MV. Expression and modulation of specific, high affinity binding sites for erythropoietin on the human erythroleukemic cell line K562. Blood. 1988; 71:104–9. [PubMed: 2825843]

19. Kirschner KM, Baltensperger K. Erythropoietin promotes resistance against the Abl tyrosine kinase inhibitor imatinib (STI571) in K562 human leukemia cells. Mol Cancer Res. 2003; 1:970–80. [PubMed: 14638869]
20. Kentsis A, Reed C, Rice KL, Sanda T, Rodig SJ, Tholouli E, et al. Autocrine activation of the MET receptor tyrosine kinase in acute myeloid leukemia. Nat Med. 18:1118–22. [PubMed: 22683780]
21. Jun YW, Sheikholeslami S, Hostetter DR, Tajon C, Craik CS, Alivisatos AP. Continuous imaging of plasmon rulers in live cells reveals early-stage caspase-3 activation at the single-molecule level. Proc Natl Acad Sci U S A. 2009; 106:17735–40. [PubMed: 19805121]
22. Tsai J, Lee JT, Wang W, Zhang J, Cho H, Mamo S, et al. Discovery of a selective inhibitor of oncogenic B-Raf kinase with potent antimelanoma activity. Proc Natl Acad Sci U S A. 2008; 105:3041–6. [PubMed: 18287029]
23. Sondergaard JN, Nazarian R, Wang Q, Guo D, Hsueh T, Mok S, et al. Differential sensitivity of melanoma cell lines with BRAFV600E mutation to the specific Raf inhibitor PLX4032. J Transl Med. 8:39. [PubMed: 20406486]
24. Sala E, Mologni L, Truffa S, Gaetano C, Bollag GE, Gambacorti-Passerini C. BRAF silencing by short hairpin RNA or chemical blockade by PLX4032 leads to different responses in melanoma and thyroid carcinoma cells. Mol Cancer Res. 2008; 6:751–9. [PubMed: 18458053]
25. Joseph EW, Pratilas CA, Poulikakos PI, Tadi M, Wang W, Taylor BS, et al. The RAF inhibitor PLX4032 inhibits ERK signaling and tumor cell proliferation in a V600E BRAF-selective manner. Proc Natl Acad Sci U S A. 2010; 107:14903–8. [PubMed: 20668238]
26. Corbin AS, Agarwal A, Loriaux M, Cortes J, Deininger MW, Druker BJ. Human chronic myeloid leukemia stem cells are insensitive to imatinib despite inhibition of BCR-ABL activity. J Clin Invest. 121:396–409. [PubMed: 21157039]
27. Traer E, MacKenzie R, Snead J, Agarwal A, Eiring AM, O'Hare T, et al. Blockade of JAK2-mediated extrinsic survival signals restores sensitivity of CML cells to ABL inhibitors. Leukemia. 26:1140–3. [PubMed: 22094585]
28. Hantschel O, Warsch W, Eckelhart E, Kaupe I, Grebien F, Wagner KU, et al. BCR-ABL uncouples canonical JAK2-STAT5 signaling in chronic myeloid leukemia. Nat Chem Biol. 8:285–93. [PubMed: 22286129]
29. Smith CC, Wang Q, Chin CS, Salerno S, Damon LE, Levis MJ, et al. Validation of ITD mutations in FLT3 as a therapeutic target in human acute myeloid leukaemia. Nature. 485:260–3. [PubMed: 22504184]
30. Huang da W, Sherman BT, Lempicki RA. Systematic and integrative analysis of large gene lists using DAVID bioinformatics resources. Nat Protoc. 2009; 4:44–57. [PubMed: 19131956]
31. Huang da W, Sherman BT, Lempicki RA. Bioinformatics enrichment tools: paths toward the comprehensive functional analysis of large gene lists. Nucleic Acids Res. 2009; 37:1–13. [PubMed: 19033363]
32. Sonnichsen C, Reinhard BM, Liphardt J, Alivisatos AP. A molecular ruler based on plasmon coupling of single gold and silver nanoparticles. Nat Biotechnol. 2005; 23:741–5. [PubMed: 15908940]
33. Reinhard BM, Siu M, Agarwal H, Alivisatos AP, Liphardt J. Calibration of dynamic molecular rulers based on plasmon coupling between gold nanoparticles. Nano Lett. 2005; 5:2246–52. [PubMed: 16277462]

Statement of Significance

We found that BCR-ABL can confer addiction *in vitro* by rewiring myeloid growth factor receptor signaling through establishment of MEK-dependent negative feedback. Our findings predict that deeper, more durable responses to targeted agents across a range of malignancies may be facilitated by maintaining negative feedback concurrently with oncoprotein inhibition.

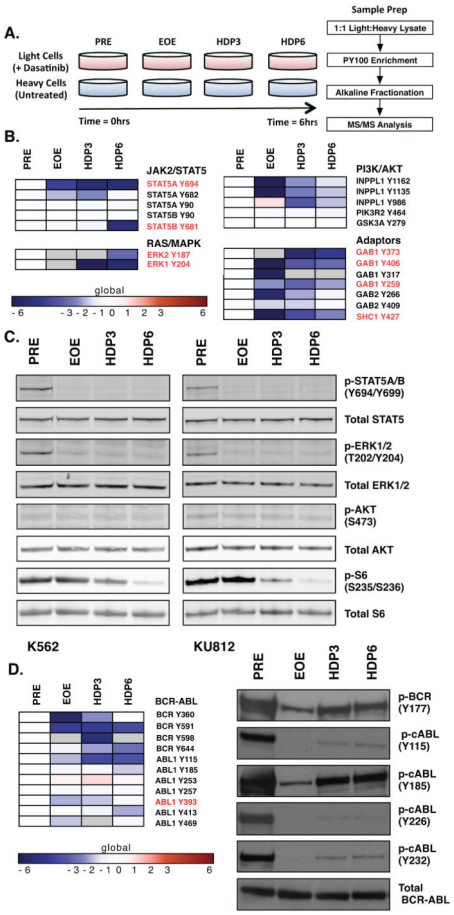

Figure 1. Transient Exposure of CML Cell Lines to Dasatinib Results in Durable Dephosphorylation of Select Tyrosine Residues in Myeloid Growth-Factor Receptor Signaling Pathways

A. Schematic of SILAC-based quantitative phosphoproteomic analysis of global phosphotyrosine signaling in the K562 cells before and after a high-dose pulse (HDP) of dasatinib. K562 cells grown in “light” (non-isotope-containing) RPMI were treated with a 100nM dasatinib for 20 minutes, and cell lysates were generated before HDP (PRE), at the time of drug washout (EOE), and 3hr and 6hrs post-HDP (HDP3, HDP6). Equivalent lysates were generated from K562 cells grown in “heavy” (isotope-containing) RPMI. Light and heavy K562 cell lysates were mixed at a 1:1 ratio prior to phosphotyrosine peptide (PY100) enrichment, peptide fractionation, and MS/MS analysis.

B. Heat map representation of persistent phosphorylation changes in myeloid growth factor receptor signaling pathways identified by bioinformatic functional analysis. Change in phosphorylation at each HDP time point was normalized to the “PRE” condition and are represented on a $\log_2$ - transformed scale. Gray areas designate “no data”.

C. Western immunoblot analysis of select myeloid growth factor receptor signaling pathways in K562 and KU812 cells before and after a 100nM HDP of dasatinib.

D. Heat map representation of BCR-ABL phosphorylation identified by phosphoproteomic analysis and western immunoblot analysis in K562 cells before and after a 100nM HDP of dasatinib. (ABL1a numbering).

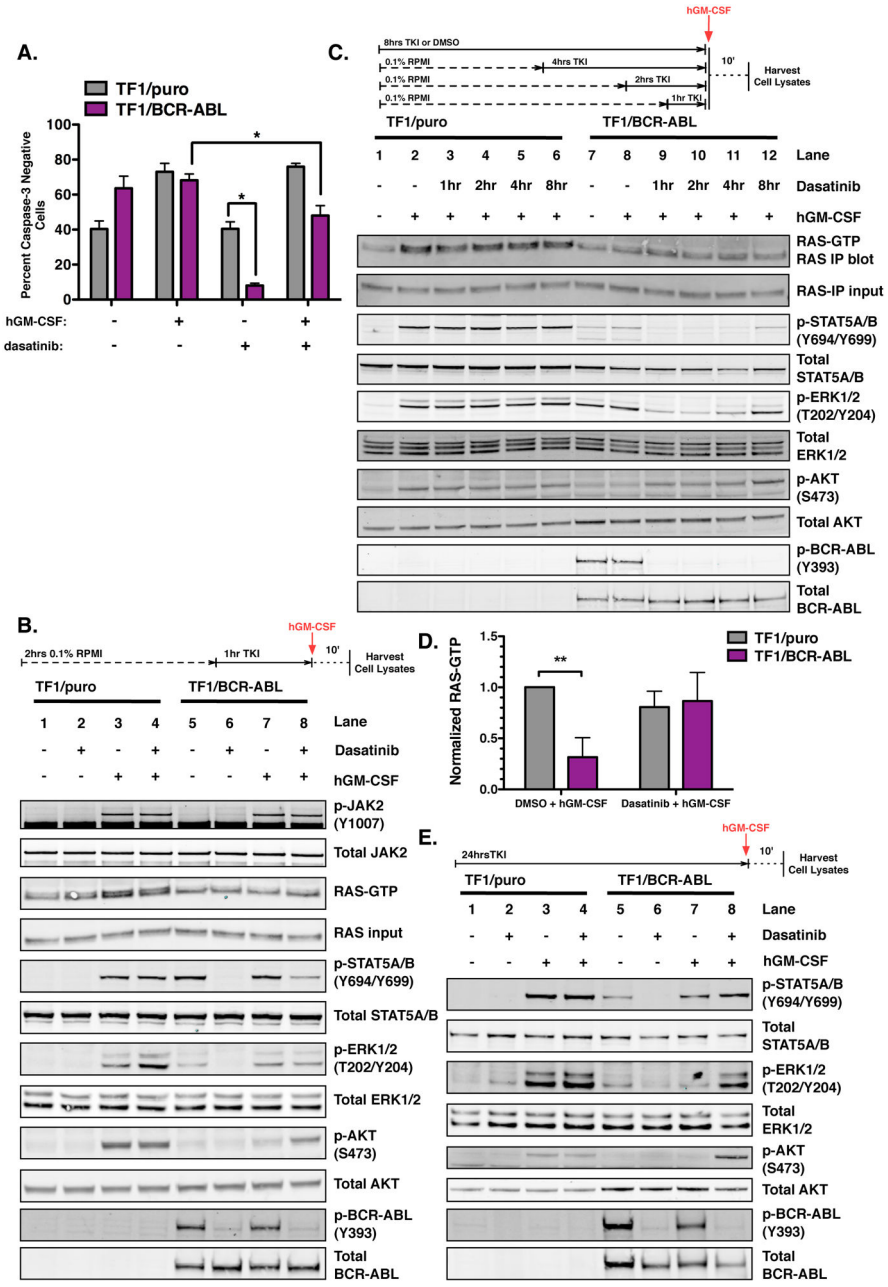

Figure 2. BCR-ABL Kinase Activity Rewires GM-CSF Receptor Signaling and Confers Oncogene Addiction in TF1 Cells

A. Percent cleaved caspase-3 negative population (live cells) of TF1/puro and TF1/BCR-ABL cells following 48 hours of treatment with, 0.2% DMSO, 2ng/mL hGM-CSF, 100nM dasatinib or 100nM dasatinib supplemented with 2ng/mL of hGM-CSF. Active caspase-3 was measured by flow cytometry. Data represent average ± SD (n=3; *p<0.001; two-way ANOVA with Bonferroni post-tests).

B. Upper: Line diagram representation of duration of serum starve, kinase inhibitor treatment, and growth-factor stimulation. Lower: Western immunoblot analysis of hGM-CSF-mediated (10′ stimulation) JAK2 activation, RAS-GTP loading, and activation of

downstream effectors from whole cell lysates in TF1/puro and TF1/BCR-ABL cells treated for 1 hour with 100nM dasatinib. The activation status of JAK2 was determined by immunoprecipitation and activation loop phosphorylation (Y1007). RAS activation was monitored using a RAS-GTP pull-down assay.

C. Upper: Line diagram representation of duration of serum starve, kinase inhibitor treatment, and growth-factor stimulation. Lower: Western immunoblot analysis of hGM-CSF-mediated (10′ stimulation) RAS-GTP loading and activation of downstream effectors in TF1/puro and TF1/BCR-ABL cells after short-term and extended dasatinib treatment (100nM: 1hr, 2hrs, 4hrs, 8hrs). RAS activity was monitored as in (B).

D. Normalized RAS-GTP loading in hGM-CSF-stimulated (10′) TF1/puro and TF1/BCR-ABL cells after prolonged dasatinib treatment (100nM, 24hrs). RAS activity was monitored as in (B). RAS-GTP loading was normalized to the level observed in the “TF1/puro - DMSO +hGM-CSF” condition for each experimental replicate. Data represent the average + SD (n=3; **p < 0.01; two-way ANOVA with Bonferroni post-tests).

E. Upper: Line diagram representation of duration of serum starve, kinase inhibitor treatment, and growth-factor stimulation. Lower: Western immunoblot analysis of whole cell lysates from TF1/puro and TF1/BCR-ABL cells after prolonged dasatinib treatment (100nM, 24hrs) and hGM-CSF stimulation (10′).

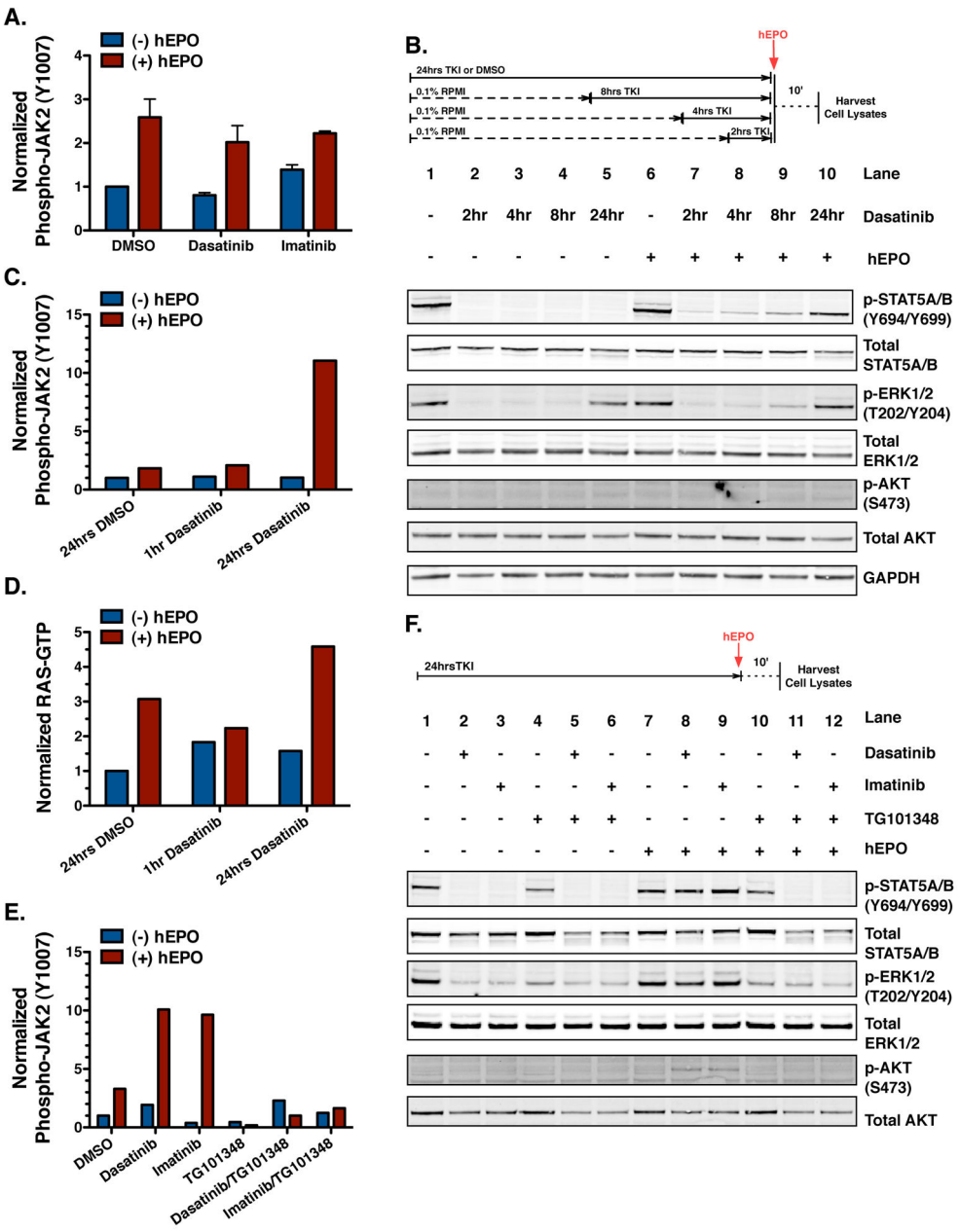

Figure 3. Erythropoietin Receptor-Mediated Activation of the JAK2/STAT5, RAS/MAPK, and PI3K/AKT Signaling Pathways is Attenuated by BCR-ABL Kinase Activity in K562 Cells

A. Normalized hEPO-mediated (10′ stimulation) JAK2 activation in K562 cells treated for 1hr with either 100nM dasatinib or 1μM imatinib. Data represents the average ± SD (n=3). JAK2 activation was monitored by immunoprecipitation and activation loop (Y1007) phosphorylation. JAK2 activation was normalized to the level of phospho-Y1007 observed in the “DMSO” condition for each experimental replicate.

B. Upper: Line diagram representation of duration of serum starve, kinase inhibitor treatment, and growth-factor stimulation. Lower: Western immunoblot analysis of whole

cell lysates from K562 cells after short-term and prolonged BCR-ABL inhibition (100nM dasatinib: 2hrs, 4hrs, 8hrs, 24hrs; 0.2% DMSO, 24hrs) followed by hEPO stimulation (10′).

C. Normalized hEPO-mediated JAK2 activation in K562 cells after short-term (1hr) and prolonged (24hrs) 100nM dasatinib treatment followed hEPO stimulation (10′). Data is representative of triplicate experimental analysis. JAK2 activation and normalization was performed as in (A).

D. Normalized RAS-GTP loading in K562 cells after short-term (1hr) and prolonged (24hrs) 100nM dasatinib treatment followed by hEPO stimulation (10′). Data is representative of triplicate experimental analysis. RAS activation was monitored using a RAS-GTP pulldown assay and RAS-GTP levels were normalized to the “DMSO” condition.

E. Normalized hEPO-mediated (10′ stimulation) JAK2 activation in K562 cells pretreated for 24hrs with 0.2% DMSO, 100nM dasatinib, 1μM imatinib, 500nM TG101348, dasatinib/TG101348, or imatinib/TG101348. JAK2 activation was monitored and normalized as in (A).

F. Upper: Line diagram representation of duration of serum starve, kinase inhibitor treatment, and growth-factor stimulation. Lower: Western immunoblot analysis of whole cell lysates in K562 cells pretreated for 24hrs with 0.2% DMSO, 100nM dasatinib, 1μM imatinib, 500nM TG101348, dasatinib/TG101348, or imatinib/TG101348 followed by hEPO stimulation (10′).

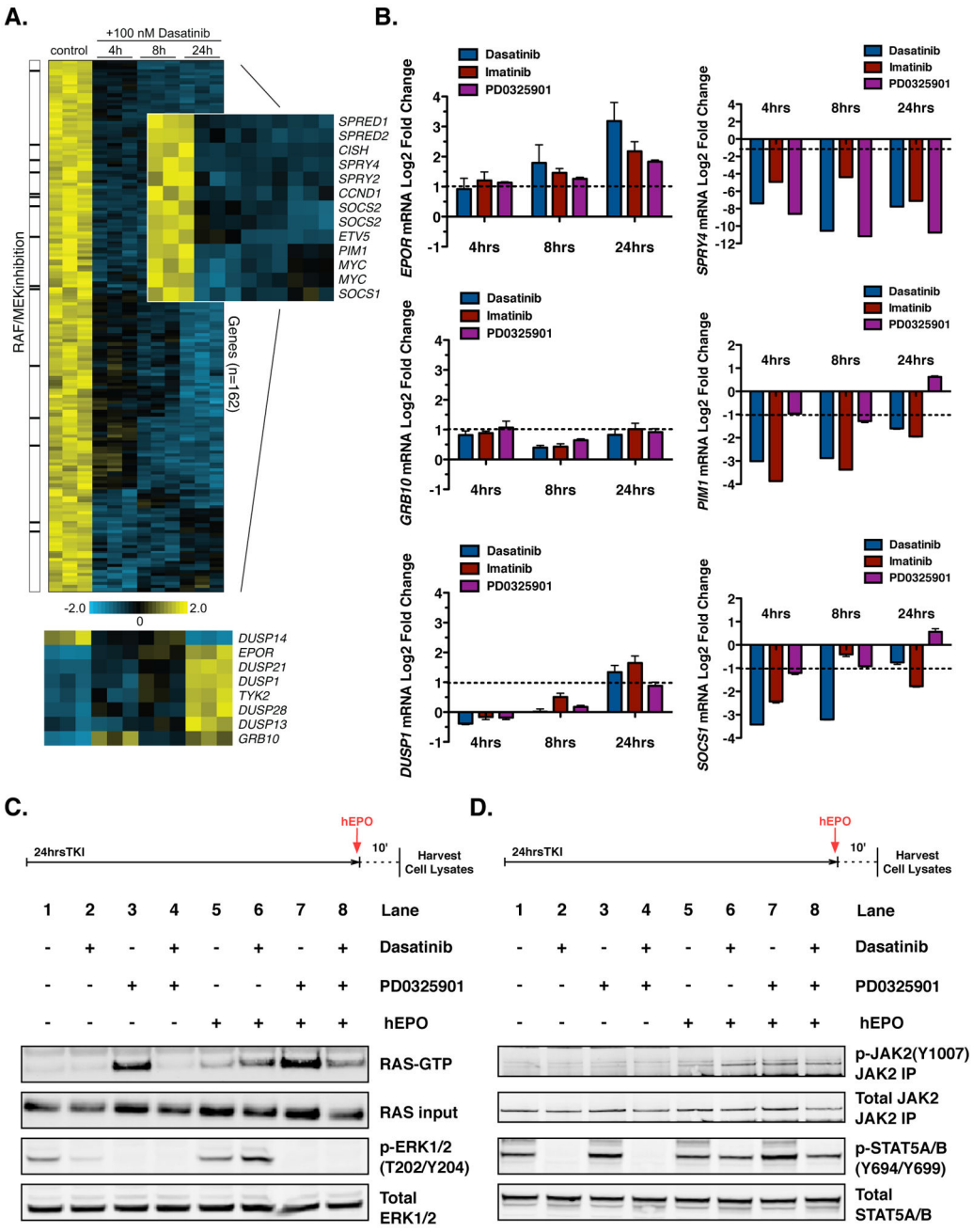

Figure 4. Global Gene Expression Analysis of Dasatinib Treated K562 Cells Identifies Candidate Mediators Responsible for the Attenuation of Myeloid GF-R Signaling in CML Cells

A. Heat map representation of the 162 genes significantly down-regulated after 4, 8, and 24 hours of dasatinib treatment in K562 cells. Heat map inset to the right highlights genes within this group that are associated with negative feedback of the RAS/MAPK and JAK/STAT signaling pathways, as well as the transcriptional output of ERK. The column to the left denotes genes previously reported to be involved in the negative feedback network of BRAFV600E expressing cells (6, 25). The heat map at the bottom highlights a few of the genes with increased expression following dasatinib treatment in K562 cells.

B. Quantitative PCR (qPCR) analysis of potential negative feedback genes in K562 cells treated with dasatinib (100nM), imatinib (1μM), or PD0325901 (500nM). The average fold expression change ($2^{(-\Delta\Delta Ct)}$) and standard deviation ($SD_{fold\text{-}change}$) for each gene is represented (n=3).

C. Upper: Line diagram representation of duration of serum starve, kinase inhibitor treatment, and growth-factor stimulation. Lower: Western immunoblot analysis of RAS and ERK activity before and after hEPO-stimulation (10′) in K562 cells pretreated for 24hrs with 0.2% DMSO, 100nM dasatinib, 500nM PD0325901, or dasatinib/PD0325901. RAS activity was monitored using a RAS-GTP pulldown assay.

D. Upper: Line diagram representation of duration of serum starve, kinase inhibitor treatment, and growth-factor stimulation. Lower: Western immunoblot analysis of JAK2 and STAT5 activity before and after hEPO-stimulation in K562 cells treated under the same experimental conditions as (A). JAK2 activation was determined by immunoprecipitation and activation loop (Y1007) phosphorylation.

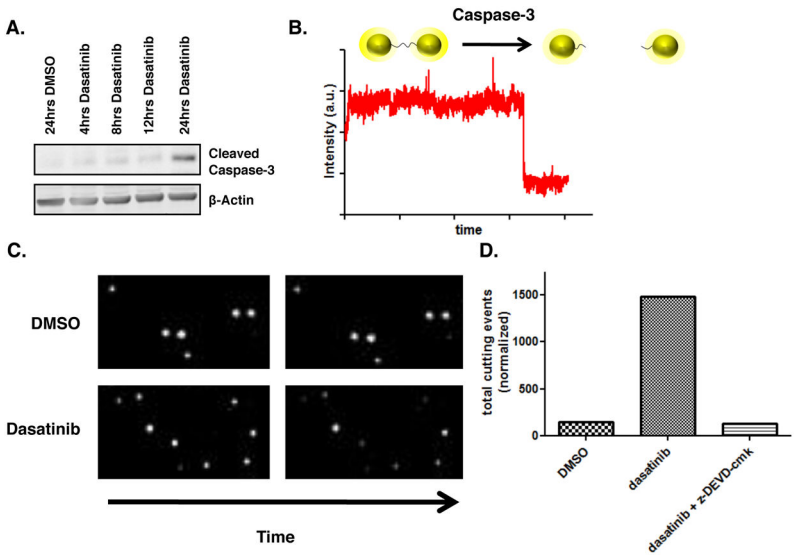

Figure 5. Caspase-3 Activity is Detected in Dasatinib Treated K562 Cells Prior to Complete Relief of Negative Feedback

A. Western immunoblot assessment of cleaved caspase-3 in whole cell lysates from K562 cells treated with 100nM dasatinib for 4hrs, 8hrs, 12hrs, and 24hrs.

B. Representation of a single gold nanosensor intensity trace as a function of time. Intact nanosensor yields a high scattering intensity, while cutting event mediated by caspase-3 is observed as an intensity drop due to loss in plasmon coupling (21, 32, 33).

C. Representative darkfield images of nanosensors before and after exposure to cell lysates from K562 cells treated with vehicle (DMSO) or 100nM dasatinib.

D. Total normalized nanosensor cutting events observed in K562 cell lysates treated with vehicle (DMSO) and 100 nM dasatinib. Treatment of lysates with the caspase-3 inhibitor z-DEVD-cmk is shown as a control.

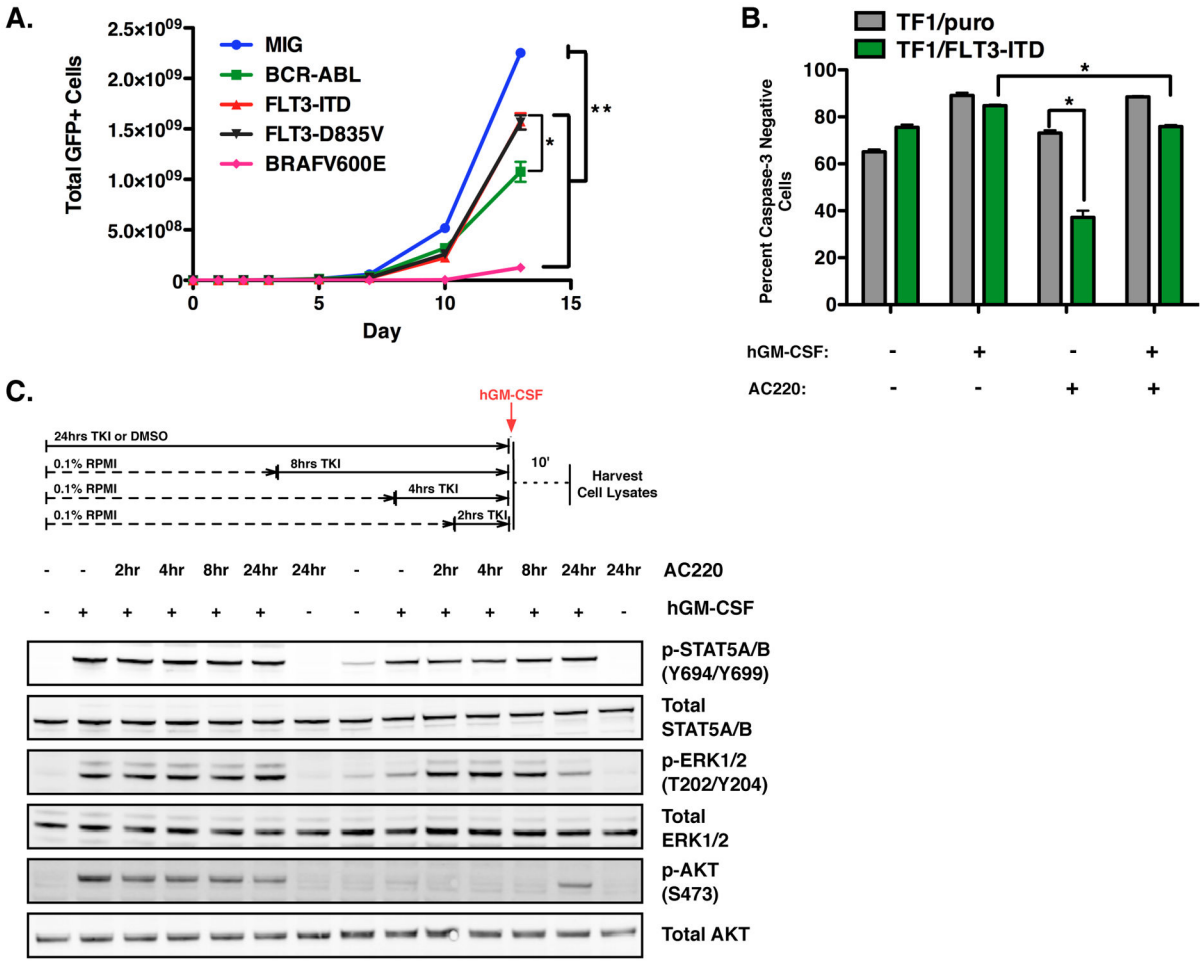

Figure 6. BCR-ABL-Dependent Negative Feedback Differs from BRAFV600E, FLT3-ITD, and FLT3-D835V in TF1 Cells

A. Growth curves of TF1 GFP-positive cells expressing BCR-ABL, BRAFV600E, FLT3-ITD, or FLT3-D835V. Cell growth in the presence of 2ng/mL hGM-CSF was monitored for 13 days. Data represents the average ± SD (n=3; *p<0.001 for p210 vs. FLT3-ITD and FLT3-D835V on day 13, **p<0.001 for MIG vs. all other cell lines on day 13. Two-way ANOVA with Bonferroni post-tests).

B. Percent cleaved caspase-3 negative population (live cells) of TF1/puro and TF1/FLT3-ITD cells following 48 hours of treatment with 2ng/mL hGM-CSF, 10nM AC220, 0.2% DMSO, or 10nM AC220 supplemented with 2ng/mL of hGM-CSF. Active caspase-3 was measured by flow cytometry. Data represent average ± SD (n=3: *p<0.001; two-way ANOVA with Bonferroni post-tests).

C. Western immunoblot analysis of TF1/puro and TF1/FLT3-ITD whole cell lysates following prolonged FLT3-ITD inhibition (10nM AC220: 2hrs, 4hrs, 8hrs, 24hrs; 0.2% DMSO, 24 hours) and hGM-CSF stimulation (10′).

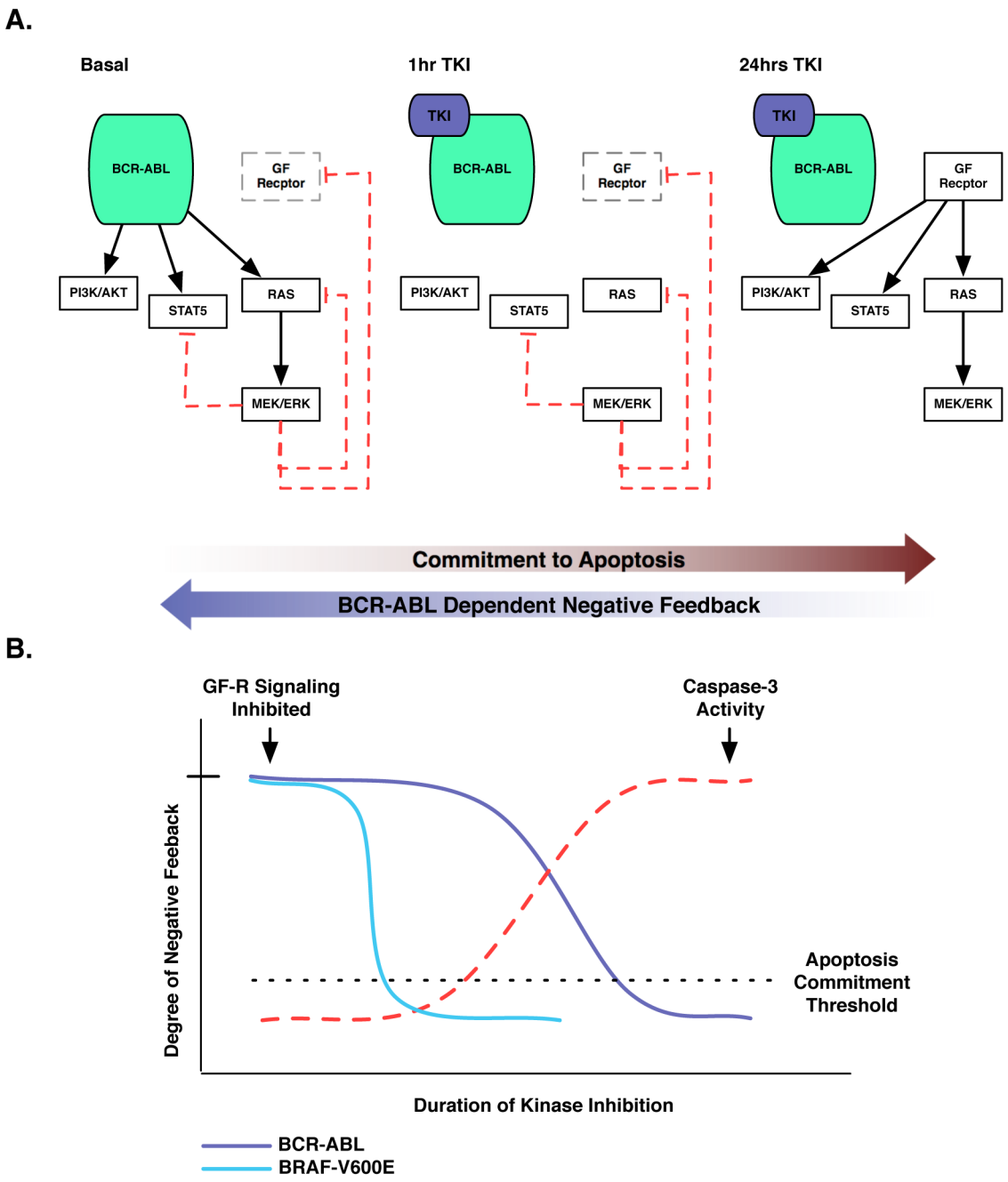

Figure 7. Model of BCR-ABL-Mediated Oncogene Addiction

A. Schematic representation of BCR-ABL-mediated oncogene addiction. BCR-ABL expressing cells initiate and commit to apoptosis prior to the complete relief of MEK-dependent negative feedback at the level of GF-R signaling.

B. Schematic comparison of the kinetics of apoptosis induction (red dashed line) and loss of negative feedback in BRAFV600E-expressing melanoma cells (cyan solid line) and BCR-ABL-expressing CML cells (blue solid line).